First publ. in: Applied Physics / A 82 (2006), 1, pp. 161-166

S. GEMMING[1]
J. TAMULIENE[1]
G. SEIFERT[1]
N. BERTRAM[2]
Y.D. KIM[2]
G. GANTEFÖR✉

Electronic and geometric structures of Mo_xS_y and W_xS_y ($x = 1, 2, 4$; $y = 1$–12) clusters

[1] Institut für Physikalische Chemie und Elektrochemie, Technische Universität Dresden, 01062 Dresden, Germany
[2] Department of Physics, University of Konstanz, 78457 Konstanz, Germany

ABSTRACT Electronic and geometric structures of M_xS_y (M = W, Mo; $x = 1, 2, 4$; $y = 1$–12) clusters have been studied using density functional theory calculations, and compared to experimental photoelectron spectra. For the metal atoms, an uptake of up to six sulfur atoms has been observed, which can be explained by the bonding of S_3^- chains. A structural difference to the corresponding oxides is the preference of bridging sites for S, which might be the origin of the differences between the structures of bulk MO_3 and MS_2. For $x = 1, 2$ the HOMO–LUMO gaps vary irregularly. For $x = 4$, a large HOMO–LUMO gap has been found for $y = 6$, 7, and 8 and the W_4S_6 and Mo_4S_6 clusters have been found to be magic with an extraordinarily high stability.

PACS 73.22.-f; 61.46.+w

1 Introduction

Inorganic nanoclusters and nanoparticles can exhibit diverse structural characteristics: on the one hand, bulk-like geometric and electronic structures can develop within a very small cluster consisting of only four metal atoms [1]. On the other hand, completely different electronic and geometric structures compared to the bulk counterparts can be found for several other nanoparticles and clusters.

Among various inorganic clusters, the properties of MX_2 (M = Mo, W; X = S, Se) have been of particular interest due to their structural similarities to carbon-based materials. As a bulk material, carbon can form a layered structure consisting of sp^2-hybridized carbon atoms. Carbon can also form nanotube structures, which can be described as folding of a graphite sheet [2]. Depending on the chirality of carbon nanotubes, a variety of electronic structures appears, and the unique properties of carbon nanotubes have attracted particular attention of scientists, under fundamental research aspects as well as for potential applications. MX_2 can also exhibit various structures and, as aforementioned, some are related to the structures of the carbon-based materials: layered structures can be found for MX_2 bulk crystals, and MX_2 nanotubes as well as fullerene-like structures of MX_2 have recently been discovered [3–6]. In addition to the carbon-like structures, a large 4–7 nm sized planar geometry and a flower-like structure have been found for MX_2, which have not been observed for the carbon-based materials so far [7, 8]. MX_2 structures are also of interest for potential applications: the MoS_2 and WS_2 polyhedral particles have been shown to be excellent lubricants, even under strongly oxidizing environments. MX_2 nanoparticles might also be useful in various tribological applications due to their exceptionally high chemical stabilities and low surface energies [9].

In contrast to the relatively large MX_2 nanoparticles, the existence of fullerene-like MX_2 structures consisting of less than 1000 metal atoms is questionable. One may expect that the inorganic fullerene structures with a diameter below 1 nm are not stable, since the dangling bonds at the edges of the MX_2 nanoplatelets can be saturated by excess S or Se atoms, stabilizing the planar structures instead of the fullerene-like ones [10]. In addition to that, the strain energy related to bending the sheet into a cage-like structure is considerably larger than in the case of carbon, as has been shown for the corresponding tubes of MX_2 [3]. In fact, recent scanning tunneling microscopy studies revealed planar triangular structures consisting of 21 Mo atoms and 48 S atoms [11].

In the present work, we studied M_xS_y ($x = 1, 2, 4$; $y = 1$–12; M = Mo, W) clusters by means of anion photoelectron spectroscopy (PES) and by density functional theory (DFT) calculations to shed light onto the elementary steps of the growth mechanisms of MX_2 nanostructures and their electronic and geometric structures. In this size regime, each additional Mo and S atom can drastically change the electronic and geometric structures of the clusters.

2 Technical details

The theoretical calculations were performed on the Mo_xS_y system only. In general, only small differences in geometric and electronic structures are expected between the Mo_xS_y and W_xS_y clusters [3, 14]. A qualitative agreement between photoelectron spectra of Mo_xS_y and W_xS_y is seen in Fig. 9. We used the generalized gradient approximation for the exchange-correlation potential in the density functional theory (DFT) as described by Becke's three-parameter hybrid functional using the non-local correlation provided by Lee, Yang, and Parr (commonly referred to as B3LYP). The 6-311G** basis set for S and the 3-21G** basis set for Mo have been used. The structures of both neutral and anionic

✉ Fax: +49-7531-885133, E-mail: gerd.gantefoer@uni-konstanz.de

clusters have been optimized globally without any symmetry constraint and by starting from various initial geometries. The Gaussian 98 program suite [12] was used for all calculations here. Due to the comparison of the Mo-sulfide structures of the theory and the corresponding experimental data of W sulfide, the quantitative argument is rather difficult. Also, the use of the restricted basis set of Mo in the theoretical calculations should also be taken into account, which can limit the quantitative analysis.

An almost complete set of experimental data has been obtained for the W_xS_y system. For the Mo_xS_y clusters, only some representative spectra have been recorded because of the difficulty of unambiguous mass separation: the mass of three sulfur atoms corresponds to the mass of one Mo atom. $Mo_xS_y^-$ and $W_xS_y^-$ clusters were produced by exposing the metal clusters to H_2S in the pulsed arc cluster ion source (PACIS) [13]. It is important to mention that exposure of the metal to H_2S at about 600 K results in the formation of MoS_2 nanostructures without H impurities [11]. The cluster temperature during the reaction of Mo and W with H_2S reagents in the PACIS is sufficiently high in order to rule out the possibility of the $M_xS_y^-$ structures being contaminated by H impurities. In addition, many photoelectron spectra of $W_xS_y^-$ clusters can be compared to the ones of $W_xO_y^-$ clusters [14] and show obvious similarities. This is also a strong argument against any H contamination. The inorganic clusters formed in the source are then cooled in the extender; at the Ultraviolet Photoelectron Spectroscopy (UPS) measurement stage, the temperature of the clusters is estimated to be room temperature. The mass of the clusters was selected by means of a time-of-flight (TOF) mass spectrometer, and the UPS spectra of the mass-selected clusters were taken with a UV laser pulse (photon energy = 6.4 and 4.66 eV).

3 Results and discussion

3.1 *Structures of* MS_y *clusters*

In Fig. 1 the optimized geometries of the neutral MoS_y ($y = 1$–6) clusters are shown. There are only marginal changes in the geometric structures of the anionic and the respective neutral clusters with the exception of MoS_4, in which the symmetry changes depending on the charge state. For MoS_y with $y = 1$–3, the Mo–S bond length grows gradually with increasing number of S atoms in the range of 2.07–2.18 Å. For MoS_4 two different Mo–S bond lengths of 2.12 and 2.48 Å have been obtained. The additional sulfur atoms in MoS_5 and MoS_6 are not directly bound to Mo; instead, they are in a bridging position between two Mo-coordinated sulfur atoms. All three S atoms together form an S_3^{2-} anion. Thus, in contrast to the bulk coordination number of six, the four-fold sulfur coordination of Mo seems to be a particularly preferable coordination environment in small Mo_xS_y species.

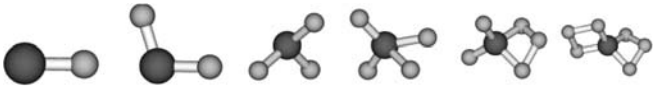

FIGURE 1 Calculated geometries of neutral MoS_y with $y = 1$–6

For MoS_5 the Mo–S bond length to the singly bound terminal S atoms is shorter (2.12 Å) than the bond length to the sulfur atoms of the trisulfide anion S_3^{2-} (2.37 Å). For MoS_6, all Mo–S bond lengths are equal at a value of 2.37 Å. MoS_y clusters with $y > 6$ have not been observed experimentally. However, clusters with up to three trisulfide groups coordinating the Mo could be obtained as stable minima on the potential energy surface. It has to be noted that clusters with $y = 7, 9$ are considerably less stable than MoS_y ($y = 1$–6), and a stable form of MoS_8 could not be found. Hence the further investigations focus on $y = 1$–6.

Figure 2a and b display mass spectra of small M_xS_y cluster anions for $x < 4$. For the MS_y series, the most intense peaks are assigned to MoS_3^-–MoS_6^- and WS_4^-–WS_6^-. There are small peaks, which can be assigned to Mo atoms and dimers reacted with oxygen; however, their intensities are much smaller than those of metal sulfide clusters. Moreover, the differences of the photoelectron spectra of sulfide clusters and corresponding oxide clusters are significant, suggesting that the concentration of the oxide clusters is negligibly small [14]. Comparing systems reacted with O and S, a pro-

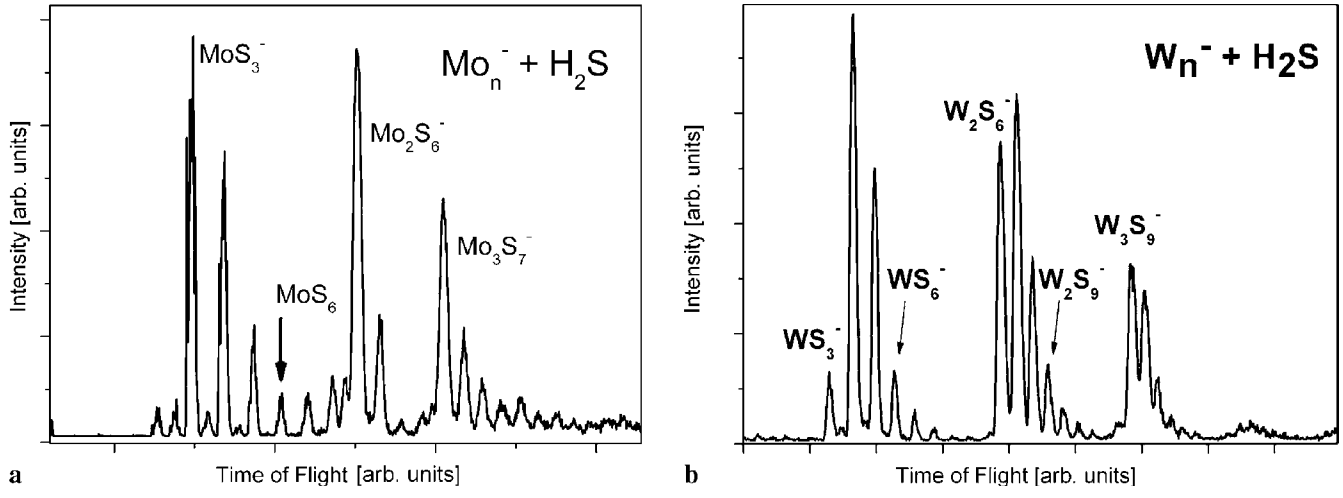

FIGURE 2 Mass spectra of small $Mo_xS_y^-$ (**a**) and $W_xS_y^-$ clusters (**b**) generated by reaction of M_n^- clusters with H_2S. In contrast to the reaction with oxygen, no indication of saturation is found

Cluster	$^2E^- - {}^1E^0$ [eV]	$^2E^- - {}^3E^0$ [eV]	$^2E^- - {}^1E^0$ (a.g.) [eV]	$^2E^- - {}^3E^0$ (a.g.) [eV]
MoS	1.37	0.4	2.5	1.28
MoS_2	2.16 (1.30*)	1.53 (0.67*)	2.28	1.64 (4.60*)
MoS_3	3.46	3.99	3.89	4.15
MoS_4	2.42	1.87	4.56	3.77
MoS_5	3.01	3.65	3.66	3.95
MoS_6	2.99	2.9	3.15	3.16

TABLE 1 Energetics of MoS_y clusters and cluster anions. ^2E is the energy of the anionic cluster. The superscript 2 indicates a doublet state. All the anionic clusters studied are in the doublet state. $^mE^0$ corresponds to the energy of the neutral cluster with a spin multiplicity, m, of a singlet ($m = 1$) or triplet ($m = 3$) state. (a.g.) indicates the anion geometry, i.e. E^2 (a.g.) is the energy of the singlet or triplet state of a neutral cluster with the same geometry as the ground-state one of the respective anionic cluster. The values with the symbol * correspond to the energy differences with the anion multiplicity of 4

nounced saturation at MO_4^- [15] has been observed for O. In the case of S no such saturation occurs and further S uptake up to MS_6^- can easily be achieved. This supports the theoretical prediction of S_3^- units (Fig. 1) being bound to the metal atom, which does not occur with oxygen.

Regarding the electronic properties of MoS_y, the MoS_2 anion exhibits two different electronic structures with dissimilar spin multiplicities; according to our calculations the quartet state is the ground state, which lies 0.86 eV below the doublet state in total energy (Table 1). It is worth mentioning that the spin multiplicity of the ground state of a cluster varies depending on the charge state: for MoS_3 and MoS_5, the singlet state is the ground state of the neutral species, whereas the other clusters occur in a triplet ground state. For MoS_4 two unpaired valence electrons at the Mo center yield the triplet ground state; hence, the formal oxidation state of Mo is +4, which is also obtained in bulk MoS_2.

The calculated vertical detachment energy (VDE) increases gradually with increasing number of S atoms in the clusters from 1 to 3, whereas a small decrease of the VDE can be found as the number of S atoms in the cluster exceeds 3 (Table 1). The adiabatic electron affinity (AEA) changes in a similar way as the VDE does (Table 1). In contrast to the changes of VDE and AEA as a function of the number of S atoms, the HOMO–LUMO gap decreases when the number

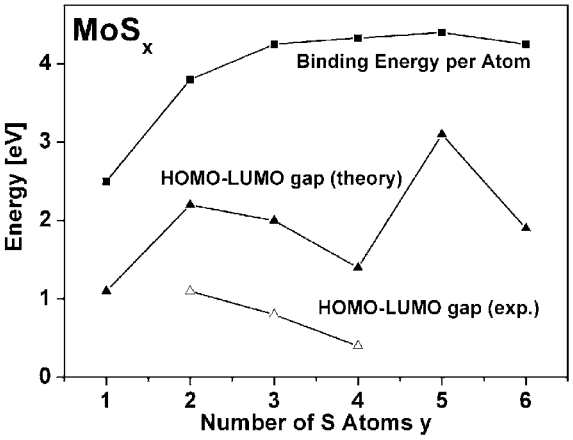

FIGURE 3 Dependence of the calculated binding energy per atom (*top trace*) and the HOMO–LUMO gaps of MoS_y on the number of S atoms y. The calculated values are plotted in the *middle trace* and compared to the experimental data (*lower trace*)

of S atoms in the cluster increases from 2 to 4 (Fig. 3). The maximum binding energy per atom has been found for $y = 5$, indicating that the MoS_5 species is the most stable one among the MoS_y clusters studied here.

Experimental photoelectron spectra (PES) were taken for MoS_y ($y = 3, 4$) and WS_y ($y = 2, 3, 4$) (Fig. 4a and b). For

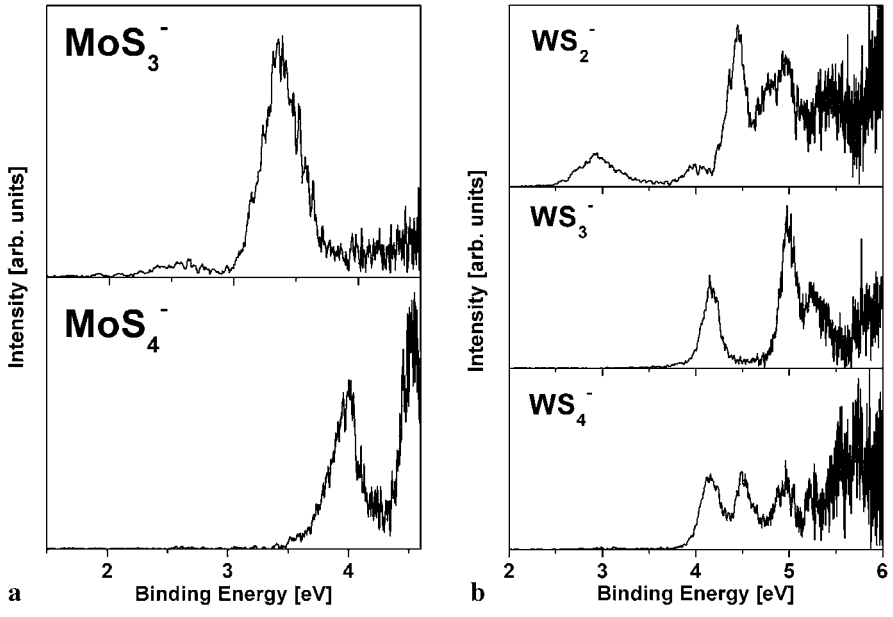

FIGURE 4 Photoelectron spectra of MoS_y^- clusters ($y = 3, 4$) recorded with a photon energy of 4.66 eV (**a**) and of WS_y^- clusters ($y = 2$–4) recorded with a photon energy of 6.4 eV (**b**)

MoS_1, MoS_2, and WS_1 the intensities were too low to record spectra, which might indicate low electron affinities in qualitative agreement with theory. The VDE of WS_2 is 2.8 eV, which is considerably higher than the value calculated for MoS_2 (Table 1). In agreement with theory, the VDEs increase to about 4 eV for $y = 4$. From Fig. 4 the HOMO–LUMO gaps of WS_2, WS_3, and WS_4 can be estimated to be 1.1 eV, 0.8 eV, and 0.4 eV, respectively.

The calculated binding energies (per atom) of the MoS_y clusters as a function of the number of S atoms in the cluster (Fig. 3) indicate that the MoS_5 cluster is the most stable species among those presented in this section. This behavior may be understood within a rather simple picture: formally, Mo reaches its largest oxidation state +6 in the case of MoS_5, where Mo is bound to two sulfide ions (S^{2-}) and one trisulfide ion (S_3^{2-}). On the contrary, in MoS_4 and MoS_6 the formal oxidation state is only +4 as in the bulk phase (MoS_2), and for lower S contents the Mo center becomes undercoordinated. In the mass spectra of the anions the most intense peaks are the ones corresponding to MS_3^- and MS_4^-. Since the intensities in mass spectra are influenced by various parameters like the growth pattern this cannot directly be compared to the calculated relative stabilities.

3.2 *Structures of* W_2S_y *clusters*

The optimized geometries of the neutral Mo_2S_y ($y = 1$–6) clusters are presented in Fig. 5. For the neutral Mo_2S_2 and Mo_2S_3 clusters, two isomers are shown, which differ in total energy by only 0.11 eV and 0.06 eV, respectively. The energy differences between these isomers are too low for a clear determination of the ground-state geometries in these cases. For Mo_2S_y with $y = 1$–3, the Mo–Mo bond length is independent of y at a value of 2.1 Å whereas, for $y > 3$, the Mo–Mo bond length rapidly increases with the number of S atoms in the cluster, resulting in a maximum Mo–Mo distance of 3 Å for Mo_2S_6 (Table 2). As in the MoS_y clusters, there are two different types of sites for the S atoms in Mo_2S_y clusters: the terminal S atoms attached to one Mo atom and the Mo–Mo-bridging S atoms. The Mo–S bond length of the terminal S atoms does not change as a function of the number of S atoms, whereas the Mo–S bond length of the bridge-bonded S atoms increases from 2.11 to 2.35 Å with increasing number of S atoms in the Mo_2S_y cluster. The formation of trisulfide ions was not observed up to $y = 6$.

Figure 6 displays a series of photoelectron spectra of W_2S_y with $y = 1$–6. No such set of spectra is available for the Mo_2S_y system. Comparing the experimental data on $W_2S_y^-$ with the calculated data on Mo_2S_y, one should keep in mind that there might be small differences in geometry and in the energetic

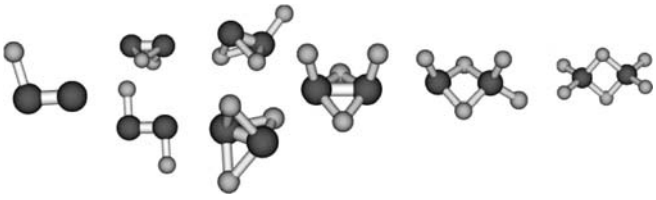

FIGURE 5 Optimized geometries of neutral Mo_2S_y clusters with $y = 1$–6

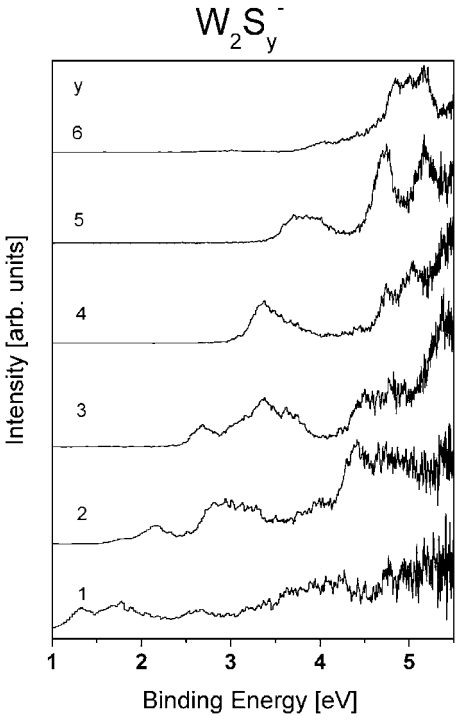

FIGURE 6 Photoelectron spectra of W_2S_y cluster anions obtained with a photon energy of 6.4 eV

positions between these two systems. The VDEs have been extracted from Fig. 6 and compared to the calculated data (Fig. 7). The VDEs increase monotonically and the agreement between theory and experiment is very favorable.

Mo_2S exhibits a calculated HOMO–LUMO gap of 1.38 eV, which is the smallest one among those of the Mo_2S_y clusters studied here (Table 2). For Mo_2S_y with $y = 2$–6, the HOMO–LUMO gap varies between 1.6 and 2.5 eV. The binding energy (per atom) rises monotonically with increasing number of S atoms in the Mo_2S_y clusters, i.e. 'saturation' does not occur at $y = 5$, as indicated for the MoS_y clusters. Mo_2S_6 is the most stable among the Mo_2S_y clusters studied here. This behavior could be rationalized by assuming that the bond strength is again correlated with the formal oxidation state of the Mo atoms. The highest oxidation state of +6 is only

Cluster	Mo–Mo bond length [Å]	Gap [eV]	$^2E^- - {}^1E^0$ [eV]	$^2E^- - {}^3E^0$ [eV]	$^2E^- - {}^1E^0$ (a.g.) [eV]	$^2E^- - {}^3E^0$ (a.g.) [eV]
Mo_2S	2.1	1.38	1.25	0.94	1.84	2.67
Mo_2S_2	2.1	1.98	2.45	1.7	2.64	3.03
Mo_2S_3	2.1	2.53	2.8	3.09	3.05	6.36
Mo_2S_4	2.7	1.64	3.23	3.14	4.69	3.78
Mo_2S_5	2.8	2.18	3.51	3.9	3.74	4.82
Mo_2S_6	3	1.87	4.36	4.82	4.87	5.59

TABLE 2 The HOMO–LUMO gaps, the Mo–Mo bond lengths, and the energy differences between various electronic states of the Mo_2S_y clusters with $y = 1$–6

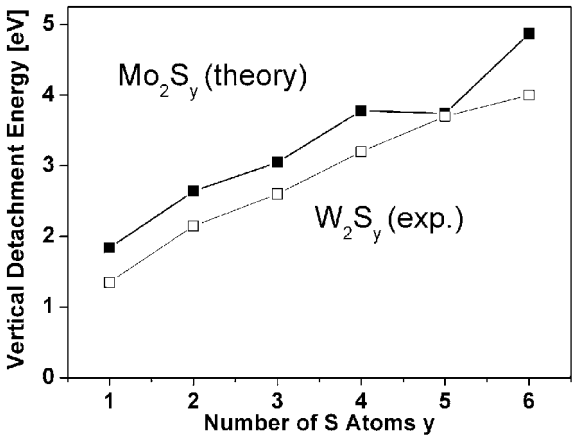

FIGURE 7 Comparison of the vertical detachment energies (VDEs) calculated for Mo_2S_y ($y = 1$–6) to the experimental VDEs for W_2S_y clusters

reached in Mo_2S_6, whereas in all other clusters ($y = 1$–5) formal *d* electrons are 'still present' at the Mo centers, which may still result in a Mo–Mo metal–metal bond. The short Mo–Mo distance for $y = 1$–3 corroborates the presence of such a bond, whereas the elongation for $y > 3$ indicates that the Mo–Mo interaction is dominated by the Mo–S–Mo bridges. Based on the high stability of the Mo_2S_6 clusters, one may suggest that the structure of Mo_2S_6 could also be a motif of larger Mo_xS_y clusters or of the bulk MoS_3 phase.

3.3 *Structures of* Mo_4S_y

The optimized geometries of the neutral Mo_4S_y ($y = 1$–12) clusters are illustrated in Fig. 8. The basic structural motif is the Mo_4 tetrahedron, which undergoes Jahn–Teller distortions towards a planar arrangement of the Mo atoms with a subsequently increasing number of S atoms up to $y = 3$. For $y = 3$, the tetrahedral Mo_4 unit is converted into an almost planar structure with two Mo–Mo bonds (2.13 Å) and two longer Mo–Mo distances (2.68 Å). The (distorted) tetrahedral Mo_4 unit is restored for the Mo_4S_y clusters with $y \geq 4$. The ideal tetrahedral Mo_4 unit is very well established for $y = 6$, where the six sulfur atoms are bridging the six edges of the Mo_4 tetrahedron. For $y > 6$ the Mo_4 tetrahedron is again distorted. In the case of Mo_4S_7 one edge is bridged by a disulfide group, whereas in Mo_4S_8 two sulfur atoms occupy terminal positions in the Mo_4 unit. With the increase of the number of sulfur atoms, i.e. an increase of the sulfur coordination number for Mo, the Mo–Mo bond is successively 'dissolved' until the maximum oxidation state of Mo is reached in the Mo_4S_{12} cluster. For almost all clusters shown here, anionic clusters and their neutral counterparts have nearly identical structures with the exception of Mo_4S_2, which shows remarkably different structures as anion and neutral species.

Figure 9a and b display the photoelectron spectra of $Mo_4S_y^-$ and $W_4S_y^-$ ($y = 1$–12) cluster anions. As one can see from Fig. 10 the calculated detachment energies correlate quite well with the binding energies of the photoemission peaks extracted from Fig. 9. Due to problems with the Self-

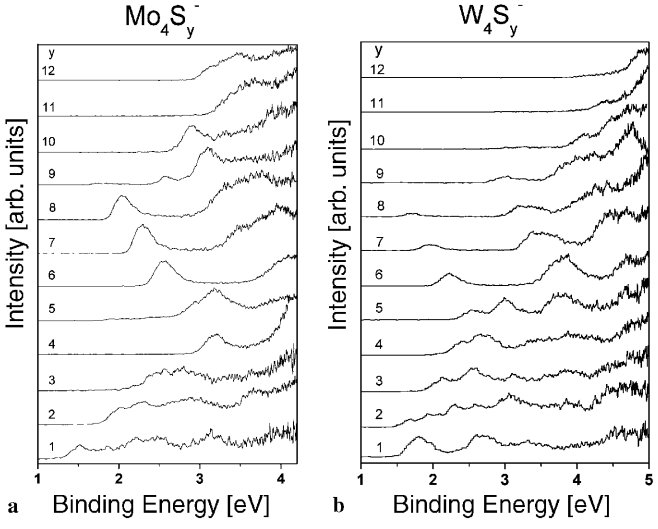

FIGURE 9 Photoelectron spectra of Mo_4S_y ($y = 1$–12) cluster anions recorded with a photon energy of 4.66 eV (**a**) and W_4S_y ($y = 1$–12) cluster anions recorded with a photon energy of 6.4 eV (**b**)

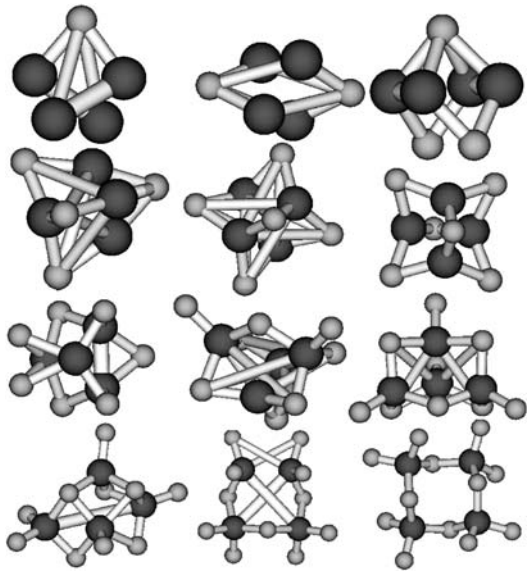

FIGURE 8 Optimized geometries of neutral Mo_4S_y clusters

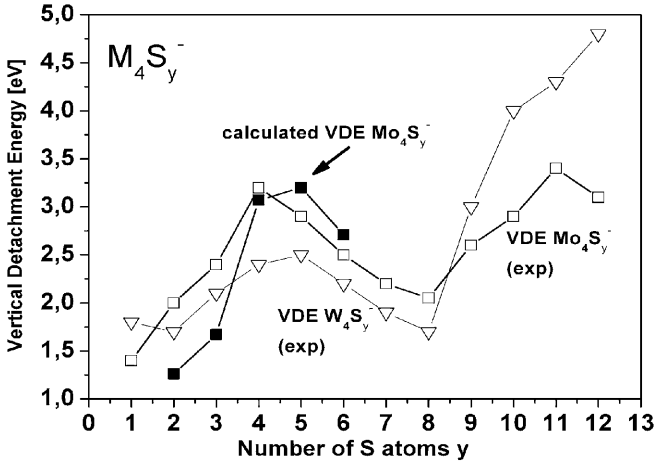

FIGURE 10 Comparison of the vertical detachment energies (VDEs) calculated for Mo_4S_y ($y = 1$–6) with the experimentally measured VDEs for $Mo_4S_y^-$ and $W_4S_y^-$ clusters

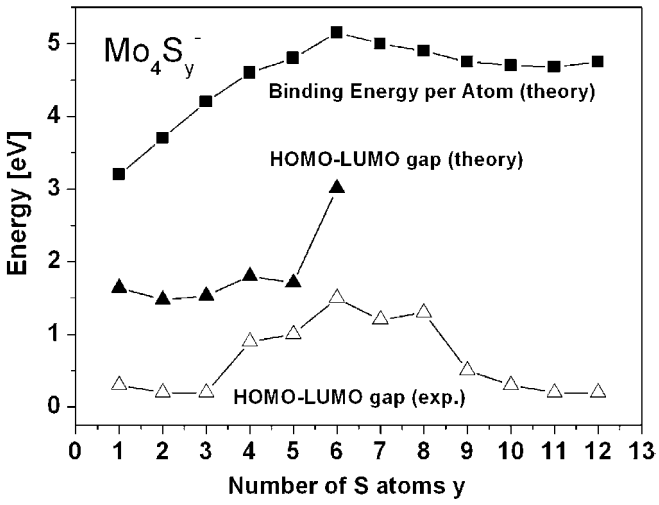

FIGURE 11 Dependence of the calculated binding energy per atom and the HOMO–LUMO gaps (calculated and measured for $Mo_4S_y^-$) on the number of S atoms

consistent field (SCF) convergence in the calculations of the cluster anions, we cannot give reliable VDEs for the clusters with $y > 6$. The appearance of a large gap between the first and second states is evident in the UPS spectra of W_4S_6 and has also been confirmed in our theoretical calculations. The HOMO–LUMO gap as a function of the number of S atoms in the Mo_4S_y clusters shows a maximum at $y = 6$.

The HOMO and the LUMO in the Mo_4S_y clusters are mainly *d* states at the Mo_4 unit of the cluster. The systematic upward shift of the first and second ionization energies for $y = 1$–5 and 9–12 may therefore qualitatively be explained by the above-mentioned 'dissolving' of the Mo–Mo bonds in the Mo_4 unit with the increasing number of sulfur atoms. The qualitative change in the spectra going from $y = 8$ to $y = 9$ may also be understood considering this behavior. In the range of $y = 6, 7, 8$ the HOMO as well as the LUMO are delocalized Mo *d* cluster orbitals. For $y > 8$ the LUMO is now localized at two Mo atoms only. The binding energy per atom also reaches a maximum for Mo_4S_6, indicating that Mo_4S_6 can be regarded as a magic cluster (Fig. 11).

In conclusion, we studied the geometric and electronic structures of small Mo_xS_y and W_xS_y clusters containing $x =$ 1, 2, and 4 atoms using density functional theory and photoelectron spectroscopy of mass-separated anions. The geometric structures are compared to the corresponding ones of the oxides, which differ in two aspects: the structures of the oxides and sulfides are different, because sulfur prefers bridge-bonding sites, while for O atoms on-top sites are also energetically allowed. Furthermore, no saturation occurs in the case of S: at higher S concentrations, S_3 chains can be bound to the metal atoms, thus enabling a much higher S uptake than in the case of oxygen.

REFERENCES

1 Q. Sun, B.K. Rao, P. Jena, D. Stolcic, Y.D. Kim, G. Ganteför, A.W. Castleman, Jr, J. Chem. Phys. **121**, 9417 (2004)
2 R. Saito, G. Dresselhaus, M.S. Dresselhaus, *Physical Properties of Carbon Nanotubes* (Imperial College Press, London 1999)
3 G. Seifert, H. Terrones, M. Terrones, G. Jungnickel, T. Frauenheim, Phys. Rev. Lett. **85**, 146 (2000)
4 M. Hershfinkel, L.A. Gheber, V. Volterra, J.L. Hutchison, L. Margulis, R. Tenne, J. Am. Chem. Soc. **116**, 1914 (1994)
5 Y. Feldman, G.L. Frey, M. Homyonfer, V. Lyakhovitskaya, L. Margulis, H. Cohen, G. Holdes, J.L. Hutchison, R. Tenne, J. Am. Chem. Soc. **118**, 5362 (1996)
6 R. Tenne, L. Margulis, M. Genut, G. Holdes, Nature **360**, 444 (1992)
7 J.M. Huang, R.A. Laitinen, D.F. Kelley, Phys. Rev. B **62**, 10995 (2000)
8 Y.B. Li, Y. Bando, D. Golberg, Appl. Phys. Lett. **82**, 1962 (2003)
9 L. Cizaire, B. Vacher, T. Le Mogne, J.M. Martin, L. Rapoport, A. Margolin, R. Tenne, Surf. Coat. Technol. **160**, 282 (2002)
10 G.L. Frey, S. Elani, M. Homyonfer, Y. Feldman, R. Tenne, Phys. Rev. B **57**, 6666 (1998)
11 S. Helveg, J.V. Lauritsen, E. Kagsgaard, S. Stensgaard, J.K. Norskov, B.S. Clausen, H. Topsoe, F. Besenbacher, Phys. Rev. Lett. **84**, 951 (2000)
12 M.J. Frisch, G.W. Trucks, H.B. Schlegel, G.E. Scuseria, M.A. Robb, J.R. Cheeseman, V.G. Zakrzewski, J.A. Montgomery, R.E. Stratmann, J.C. Burant, S. Dapprich, J.M. Millam, A.D. Daniels, K.N. Kudin, M.C. Strain, O. Farkas, J. Tomasi, V. Barone, M. Cossi, R. Cammi, B. Mennucci, C. Pomelli, C. Adamo, S. Clifford, J. Ochterski, G.A. Petersson, P.Y. Ayala, Q. Cui, K. Morokuma, D.K. Malick, A.D. Rabuck, K. Raghavachari, J.B. Foresman, J. Cioslowski, J.V. Ortiz, B.B. Stefanov, G. Liu, A. Liashenko, P. Piskorz, I. Komaromi, R. Gomperts, R.L. Martin, D.J. Fox, T. Keith, M.A. Al-Laham, C.Y. Peng, A. Nanayakkara, C. Gonzalez, M. Challacombe, P.M.W. Gill, B.G. Johnson, W. Chen, M.W. Wong, J.L. Andres, M. Head-Gordon, E.S. Replogle, J.A. Pople, *Gaussian 98*, rev. A.7 (Gaussian Inc., Pittsburgh, PA 1998)
13 S. Burkart, N. Blessing, B. Klipp, J. Müller, G. Ganteför, G. Seifert, Chem. Phys. Lett. **301**, 546 (1999)
14 N. Bertram, Y.D. Kim, G. Ganteför, Q. Sun, P. Jena, J. Tamuliene, G. Seifert, Chem. Phys. Lett. **396**, 341 (2004)
15 D. Stolcic, Y.D. Kim, G. Ganteför, J. Chem. Phys. **120**, 5 (2004)